# 1

# Implementation of an Active Suspension, Preview Controller for Improved Ride Comfort

*M. D. Donahue  J. K. Hedrick*

**Abstract**

A fully active suspension and preview control is utilized to improve ride comfort, which allows increased travelling speed over rough terrain. Previous research is extended and the relevant implementation issues are addressed. Specifically, the methodology of model predictive control has been applied to explicitly address suspension saturation constraints, suspension rate limits, and other system non-linearities. For comparison, the following non-preview controllers were implemented: a skyhook damping controller, a linear quadratic regulator, and a mock passive suspension controller. Particular attention is given to the hydraulic actuator force controller that tracks commands generated by higher-level controllers. The complete system has been successfully realized on a US military high-mobility multi-purpose wheeled vehicle (HMMWV) using a commercially available microprocessor platform. Experimental results show that the power absorbed by the driver is decreased by more than half, significantly improving ride comfort.

## 1.1 Introduction

Significant attention has been paid to the design of active and semi-active vehicle suspensions. This paper focuses on implementation of an active suspension; where, the standard shock absorbers of the passive suspension are replaced with rectilinear hydraulic actuators governed by electrohydraulic servovalves. The overall objective is to improve ride comfort and maintain crisp handling. Active suspensions can modulate the flow of energy to and from the system [13]. Furthermore, the dynamic characteristics of an active suspension can be continuously adjusted in response to driving conditions as measured by sensors mounted on the vehicle, allowing for better resolution of the trade-offs between ride comfort and road holding [7].

Prevalent techniques used for the design of active suspension controllers [9] require that vehicle actuators track a desired input force trajectory. In this paradigm, there are two distinct, interesting research topics: how to control the actuator to obtain the desired force and how to generate the desired force trajectory.

Several authors who have considered the force generation process of the electrohydraulic servosystem for active suspension control [5], [16] warn that ignoring the nonlinear effects of the actuator dynamics could lead to system instability. Prior attempts at classical control solutions to the force tracking problem have proved incapable of producing adequate results [2]. This has made the design and implementation of more complex, nonlinear control algorithms, such as sliding mode control methods [3], [12], a necessity to achieve acceptable performance.

As explained by Alleyne and Liu [4], the inadequacy of simple methods to solve this problem stems from fundamental limitations in the basic force tracking formulation. The absence of a pure damping element in the system, *i.e.* a shock absorber, and the inherent feedback of the piston velocity to the actuator chamber pressure, (1.3), result in a pair of lightly damped zeros on the open-loop force transfer function. These zeros cannot be modified by simple feedback and produce severe bandwidth restrictions on the force tracking controller. Osorio *et al* [10] present an output redefinition solution to this problem. An artificial damping term is added to the system dynamics, making it possible to better damp the zerodynamics of the system.

Approaches to determine the desired force trajectory include skyhook damping and linear quadratic regulators. More interesting, is the potential to use information of the upcoming road and theoretical system models to compute an optimal force trajectory. Tomizuka [17], Hac [8], and Thomson *et al* [15] present possible solutions. However, the method of model predicative control, as discussed by Gopalasamy *et al* [6], will be used here as it explicitly considers system constraints and nonlinearities.

This work combines the findings of previous researchers and implements an active suspension, preview controller on a commercially available microprocessor platform. Experiments to evaluate the performance of the controllers are conducted on a specially equipped, US military HMMWV. The

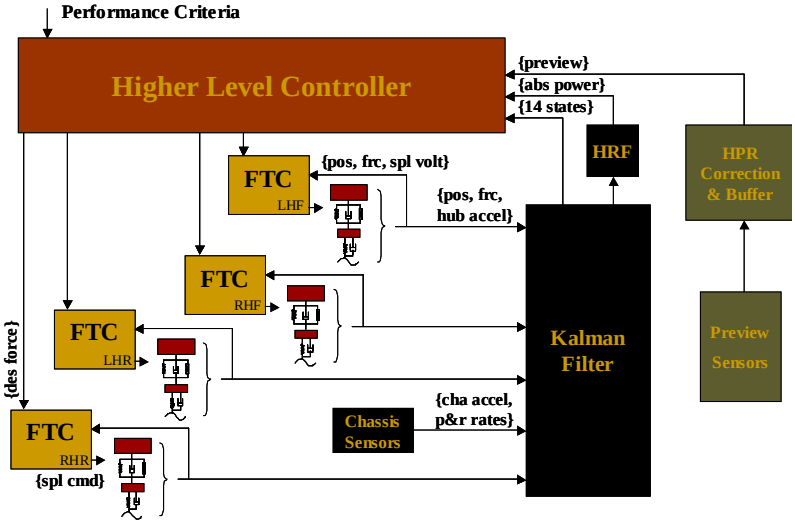


**Figure 1.1** Controller system structure, 22 sensors required

vehicle is outfitted with hydraulic actuators, a sensor suite to measure system states, and two preview sensors. More information is provided in Appendix 1.A.

Section 1.2 provides an overview of the control structure. Section 1.3 presents the force tracking controller models and control law derivation. Section 1.4 outlines the different higher-level controller paradigms. Section 1.5 explains the preview correction algorithms. Section 1.6 describes the experimental set-up and presents the experimental results.

## 1.2 Controller Structure

A hierarchical control structure is used. There are four inner control loops, one outer control loop, and several supporting subsystems, Figure 1.1. Four independent force-tracking controllers (FTCs) operate on quarter-car systems using raw sensor data for feedback signals. The Kalman filter combines sensor information into one consistent set of state information. A higher-level controller operates on this information and generates the desired force for the FTCs. Only one type of higher-level control is active at a given time. The higher-level controllers are updated at a slower sampling rate than the FTCs. Preview information is gathered, corrected and buffered until requested by a higher-level controller.

## 1.3 Force Tracking Controller

The force tracking controller, Figure 1.2, regulates the force of an individual actuator to the desired force prescribed by a higher-level controller.

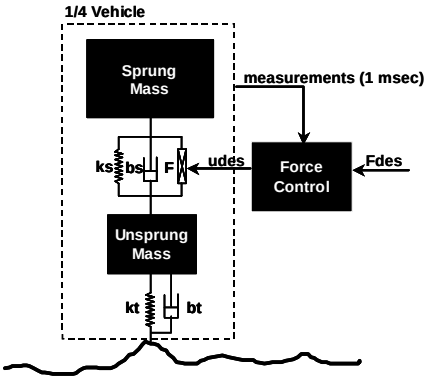


**Figure 1.2** Diagram of force tracking controller system and quarter-car model

Although the higher-level controller may make decisions based upon the full car model, it is sufficient to only consider the quarter car dynamics when designing a controller for a single actuator. For the actual system, the added dynamics due to full car motion may be considered as model errors. This and other implementation issues are addressed following the controller derivation.

## Plant Models

***Quarter-car.*** A standard quarter-car model is used (1.1), see Figure 1.2 and Appendix 1.C for the respective schematic and nomenclature. One item to note is the existence of a pure damping element in parallel with the hydraulic actuator. In a typical application, the shock is removed. However, the model behaves closer to the actual system when a pure, low damping coefficient, damping element is used.

$$\begin{aligned}\Sigma F_{ms} &= c_s(\dot{x}_u - \dot{x}_s) + k_s(x_u - x_s) + F_a - F_f \\ &= m_s\ddot{x}_s \\ \Sigma F_{mu} &= c_t(\dot{r} - \dot{x}_u) + k_t(r - x_u) + k_s(x_s - x_u) \\ &\quad + c_s(\dot{x}_s - \dot{x}_u) - F_a + F_f \\ &= m_u\ddot{x}_u\end{aligned} \tag{1.1}$$

It is convenient to define the state space, state vector as follows:

$$\beta = [r - x_u, \dot{x}_u, x_u - x_s, \dot{x}_s] \tag{1.2}$$

***Hydraulic actuator.*** The hydraulic actuators are governed by electrohydraulic servovalves and are mounted in parallel to the suspension springs, allowing for the generation of forces between the sprung and unsprung masses.

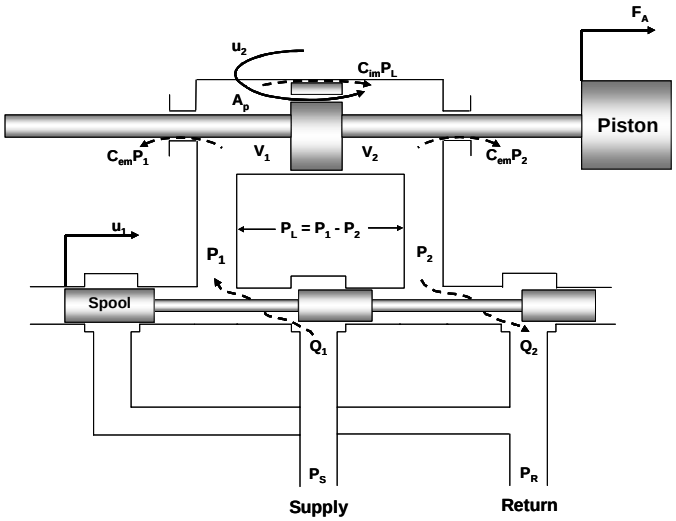


**Figure 1.3** Physical schematic and variables for the hydraulic actuator

The electrohydraulic system consists of an actuator, a primary power, spool valve, and a secondary bypass valve. As seen in Figure 1.3, the hydraulic actuator cylinder lies in a follower configuration to a critically centered electrohydraulic power spool valve with matched and symmetric orifices. Positioning of the spool $u_1$ directs high-pressure fluid flow to either one of the cylinder chambers and connects the other chamber to the pump reservoir. This flow creates a pressure difference $P_L$ across the piston. This pressure difference multiplied by the piston area $A_p$ provides the active force $F_A$ for the suspension system.

Dynamics for the hydraulic actuator [11] valve are given below. Parameter definitions and experimental values are given in Appendix 1.C. The change in force is proportional to the position of the spool with respect to center, the relative velocity of the piston, and the leakage through the piston seals. A second input $u_2$ may be used to bypass the piston component by connecting the piston chambers.

$$\dot{F}_A = A_p\alpha[C_{d1}wu_1\sqrt{\frac{P_s - \text{sgn}(u_1)P_L}{\rho}} - C_{d2}u_2\,\text{sgn}(P_L)\sqrt{\frac{2|P_L|}{\rho}} - C_{tm}P_L - A_p(\dot{x}_s - \dot{x}_u)] \tag{1.3}$$

The bypass valve $u_2$ could be used to reduce the energy consumed by the system. If the spool position $u_1$ is set to zero, the bypass valve and actuator will behave in a similar fashion to a variable orifice damper. For the purposes of this work, the bypass valve input $u_2$ is set to zero during experiments.

Spool valve positions $u_1$ and $u_2$ are controlled by a current-position feedback loop. The essential dynamics of the spool, Equation (1.4), have been shown to resemble a first order system forced by a voltage for frequencies less than 15 Hz [4].

$$\tau\dot{u} + u = kv \tag{1.4}$$

***Complete system.*** The system to be controlled by the FTC is the combined quarter-car plant and hydraulic actuator; spool voltage, $V$, is the control input. Defining the state $x_5 = P_L = F_A/A_p$ and choosing the state vector of Equation (1.5), the state space representation of the system can be written as in Equation (1.6). Suspension friction and road disturbance are considered model errors and are not shown.

$$X = [r - x_u, \dot{x}_u, x_u - x_s, \dot{x}_s, \frac{F_A}{A_p}, u_1] \tag{1.5}$$

$$\dot{X} = \begin{bmatrix} 0 & -1 & 0 & 0 & 0 & 0 \\ \frac{k_t}{m_u} & -\frac{c_t+c_s}{m_u} & \frac{-k_s}{m_u} & \frac{c_s}{m_u} & \frac{-A_p}{m_u} & 0 \\ 0 & 1 & 0 & -1 & 0 & 0 \\ 0 & \frac{c_s}{m_s} & \frac{k_s}{m_s} & \frac{-c_s}{m_s} & \frac{A_p}{m_s} & 0 \\ 0 & A_p\alpha & 0 & -A_p\alpha & -\alpha C_{tm} & 0 \\ 0 & 0 & 0 & 0 & 0 & \frac{-1}{\tau} \end{bmatrix} X + \begin{bmatrix} 0 \\ 0 \\ 0 \\ 0 \\ \Phi \\ 0 \end{bmatrix} + \begin{bmatrix} 0 \\ 0 \\ 0 \\ 0 \\ 0 \\ \frac{k}{t} \end{bmatrix} V \tag{1.6}$$

where $\Phi = \alpha C_d w x_6 \sqrt{\frac{P_s - \mathrm{sgn}(x_6)x_5}{\rho}}$

## Control Algorithms

As seen in Equation (1.6), there is a severe non-linearity $\Phi$ in the dynamic behavior of the system. The most direct approach to solving this problem is dynamic surface control [2].

***Dynamic surface control.*** For the system in Equation (1.6), the control enters through the spool voltage. Applying dynamic surface control as described by Slotine and Li [14], the output $F_A$ was differentiated with respect to time until the control input appeared. The resulting system has relative degree 2 and 4 internal dynamic states. The controller surfaces are

$$P_L = \frac{F_A}{A_p} \quad \text{and} \quad u_{spool} \tag{1.7}$$

For the $P_L$ surface, an integral term was added to the standard definition of $s$. The integral term, weighted by $0 < \lambda_1 < 1$, slightly attenuates control noise.

$$s_1 = \tilde{x}_5 + \lambda_1 \int \tilde{x}_5 dt \qquad \text{where } \tilde{x}_5 = x_5 - x_{5d} \tag{1.8}$$

Applying the sliding surface approach, the control law must satisfy the condition in Equation (1.9) to ensure asymptotic tracking of $F_{des}$.

$$s_1\dot{s}_1 = s_1(\dot{\tilde{x}}_5 + \lambda\tilde{x}_5) \leq -\eta_1 s_1^2 \tag{1.9}$$

Plugging in the equation of dynamics for $\dot{x}_{5d}$ and solving for $u_{des}$:

$$u_{des} = \frac{1}{\Phi}\{A_p\alpha(x_4 - x_2) + \alpha C_{tm}x_5 + \dot{x}_{5d} - \lambda_1\tilde{x}_5 - \eta_1 s_1\} \tag{1.10}$$

In Equation (1.10), the desired force profile enters through the terms $\dot{x}_{5d}$ and $s_1$. Because the time derivative of the desired force is used in control computation, it is important for the force profile to be smooth.

Following the method used for the $P_L$ surface, the equation for control input $V$ can be obtained as follows:

$$\begin{aligned} s_2 &= u - u_{des} \\ s_2\dot{s}_2 &= s_2(\dot{u} - \dot{u}_{des}) \leq -\eta_2 s_2^2 \end{aligned} \tag{1.11}$$

Substituting the equation of dynamics for $\dot{u}$ into Equation (1.11) and solving, the control input is thus:

$$V = \frac{1}{k}\{u + \tau\dot{u}_{des} - \eta_2\tau s_2\} \tag{1.12}$$

The time derivative of $u_{des}$ is needed to compute the control input $V$. Using the filter of Equation (1.13) allows theoretical proof that the resulting controller is asymptotically stable.

$$\dot{\Psi} = \frac{u_{des} - \Psi}{\tau} \tag{1.13}$$

Note that $\dot{\Psi}$ is used in place of $\dot{u}_{des}$ in Equation (1.12). The state $\Psi$ is maintained via forward Euler integration of $\dot{\Psi}$.

In theory, choosing the sliding surface gains to overcome the worst-case model and disturbance errors ensures asymptotic tracking of the desired profile.

Output redefinition reduces model errors by directly considering the lack of a pure damping element in the system [10]. Other methods that afford increased gains are presented in the following section.

**Implementation**

The desired spool position command output by the first surface, $P_L$, is very noisy. The second surface amplifies the noise and causally decreases sliding mode gains. It was empirically determined that the filter in Equation (1.14) reduced control noise and improved controller performance. With this filter,

$u'_{des}$ replaces the $u_{des}$ command sent to the second surface in Equation (1.11).

$$u'_{des} = \frac{u_{des}(k-1) + u_{des}(k-2)}{2} \tag{1.14}$$

Another empirical study showed that numerical differentiation, Equation (1.15), of $\dot{u}_{des}$ worked better than the sliding mode filter described in Equation (1.13).

$$\dot{w}_{des}(k) = \frac{w_{des}(k) - w_{des}(k-1)}{\Delta t} \tag{1.15}$$

***Model error filters.*** The FTC formulation above treats the full car dynamics as a disturbance. Results indicate that FTC performance around the resonant chassis modes is poor. Resonant frequency for the pitch and heave modes is around 2 Hz and around 4 Hz for the roll mode. Attenuating the $u_{des}$ command inputs near these frequencies improves force tracking. To implement these filters with high-level controller force generation a heave, pitch, and roll quantification scheme was used. Ultimately, FTC tuning was sufficient as to eliminate the need for these filters. Moreover, a model predictive control (MPC) formulation considers these resonant frequencies when computing $F_{des}$.

***Higher-level controller filters.*** Hierarchical control inputs are generated at a slower sampling rate (30 ms due to processor constraints) than the 1 ms FTC task. A 1 ms sampling rate is necessary to ensure good tracking up to 8 Hz as dictated by the system time constants. For smooth convergence to $F_{des}$, considering the derivative terms in Equation (1.10), the desired force was filtered by Equation (1.16). A plot of the filter step response is shown in Figure 1.4, the rise time is approximately 27 ms.

$$\hat{F}_{des}(s) = \frac{6.4e9}{s^4 + 950s^3 + 385625s^2 + 7.6e7s + 6.4e9} \tag{1.16}$$

## 1.4 Higher-level Controllers

Higher-level controllers compute the desired force for the four independent FTCs. Controllers have access to the vehicle information listed below. The bold items are states provided by a 14 state Kalman filter (KF) operating on a 7 degree-of-freedom (DOF) full car model.

- **Suspension Expansion**, Suspension velocity;
- **Hub Velocity**;
- **Tire Deflection**;
- **Chassis Pitch and Roll rate**, Chassis HPR.

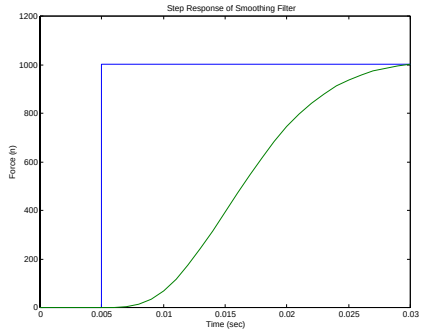


**Figure 1.4** Plot of $F_{des}$ smoothing filter step response

### Zero Force

The desired force is set to zero. This controller is a very simple attempt to reduce suspension acceleration.

### Skyhook Damping Controller

Four independent skyhook dampers are implemented on the HMMWV, one for each wheel. The plant dynamics are derived from those of a modified quarter-car model. For skyhook damping, a theoretical damper is used to reduce the velocity of the sprung mass. The control law is given by Equation (1.17), [1].

$$F_{des} = -B_{sky}\dot{x}_s + K_{vel}(\dot{x}_u - \dot{x}_s) \tag{1.17}$$

Controller gains are chosen to adjust the pole locations of the original system. The gain set $\{B_{sky}, K_{vel}\} = \{2000, 1000\}$ is used on the HMMWV.

### Linear Quadratic Regulator

A standard linear quadratic regulator (LQR) formulation for suspension systems is implemented. The plant dynamics are of the form used by the Kalman filter. Thus, the cost function includes

*{Chassis accel, Susp travel, Tire deflection,*
*Pitch & roll rates, Hub vel, Control usage}*

Some transformations are required to put the associated cost function into standard form and obtain the Riccati equation. Consult Thompson *et al* [16] for more details. MATLAB$^{TM}$ is used to generate the LQR optimal matrix gain K. Chassis acceleration, pitch and roll rates have the highest costs.

### Model Predictive Controller

The MPC was designed and coded for the HMMWV environment by Scientific Systems Inc., source code and libraries are implemented in SIMULINK

**Table 1.1** LQR weighting gains

| Parameter | Weight |
|---|---|
| Chassis acceleration | 10 |
| Pitch & roll rate | 10 |
| Suspension travel | 1 |
| Hub velocity | 1 |
| Tire deflection | 0.1 |
| Control usage | $1e^{-4}$ |

via S-function. MPC is the primary computation for the 300 MHz Alpha processor, at a $\Delta$t of 30 ms.

At each sampling instant, the MPC computes a finite number of future control moves such that a cost function, over a finite horizon, is minimized. The first control output is fed to the FTC. The exact workings of the MPC involve output prediction (based on a system model) and a receding-horizon approach. For more information on MPC formulation, consult Gopalasamy *et al* [6]. Therein, they describe how to recast the MPC problem to a constrained quadratic programming (QP) problem and how to select an appropriate real-time algorithm.

The superscript $_p$ denotes the usage of preview information. In other words, MPC$_p$ enhances MPC by considering $\dot{Z}_{road}$ and relative road heights for the desired preview horizon ($pH$) at each wheel.

Of interest to this project are the cost function weighting parameters and the physical constraint set, Table 1.2 and Table 1.3, respectively. Field testing of the MPC and skyhook controllers motivated the addition of an "optimal" skyhook (suspension velocity) damping term in the MPC cost function. The absorbed power term will be explained in Section 1.6.

**Table 1.2** MPC weighting gains

| Parameter | Weight |
|---|---|
| Absorbed power | 23 |
| Suspension travel | 0.02 |
| Suspension velocity | 192 |
| Tire deflection | 0.08 |
| Control usage | $1.1e^{-6}$ |

**Table 1.3** MPC constraint values

| Constraint | Value |
|---|---|
| Force | $\pm$ 8000 N |
| Force rate | $\pm$ 5000 N/s |
| Suspension travel | $\pm$ 0.06 m |

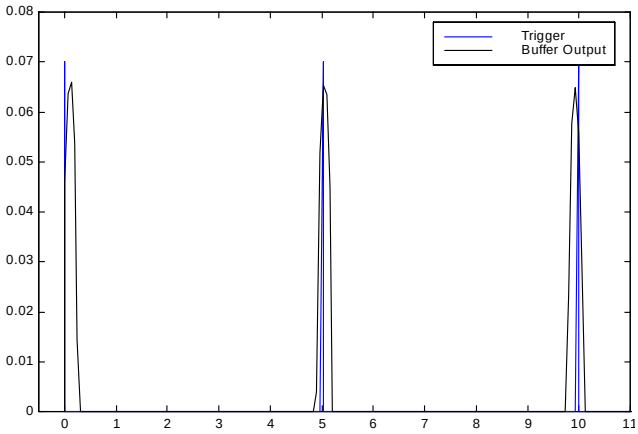


**Figure 1.5** Buffered, generated preview data matched peak loads

## 1.5 Preview Information

The $\text{MPC}_p$ requires the road profile, $Z_{road}$, and the rate that $Z_{road}$ is changing with respect to time $\dot{Z}_{road}$ for $n$ preview steps, $pH$, at each wheel. Road profiles for each side of the car are stored in a buffer. When extracting preview data, the buffer is parsed and information of the current vehicle velocity and $Z_{road}$ are combined to create $\dot{Z}_{road}$. The HMMWV system has two methods to obtain $Z_{road}$.

***Preview generation.*** Preview generation is used on courses with a known road profile, such as the test track, Appendix 1.B. The preview buffer is fed a pre-stored profile in place of the sensor preview data. The digital profile is synchronized to the actual profile using HMMWV sensors. Figure 1.5 shows a sample buffer output matched with peaks from the suspension load cells. The load triggered spikes indicate the most probable location of the actual bump. Preview generation relies on absolute position and is susceptible to error accumulation; in Figure 1.9 at 10 m the predicted bump location is no longer accurate. To contrast, preview sensor data requires at most 4 m, slightly more than the length of the vehicle.

***Preview sensors.*** On unknown terrain, we obtain preview information via sensors that measure the range to ground. Sensor measurements are converted to road height by Equation (1.18), see variable definitions in Figure 1.6. The preview sensors are rigidly attached to the chassis and have the same heave, pitch and roll (HPR). HPR are measured much faster than the rate of change of HPR and the chassis is assumed to have negligible

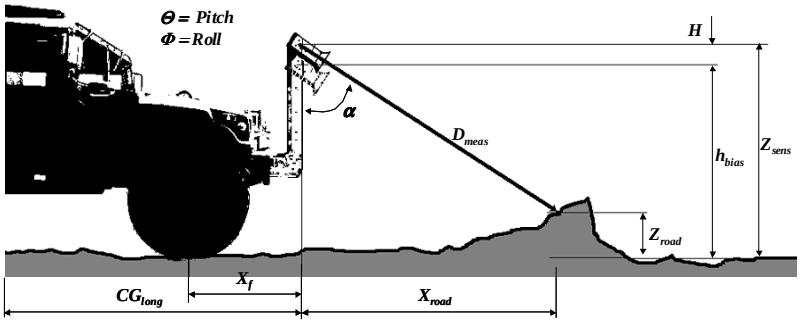


**Figure 1.6** Diagram and nomenclature definition for preview correction computation

warp. Thus, it is reasonable to directly apply trigonometry.

$$\begin{aligned} Z_{road} &= Z_{sens} - D_{meas}\cos(\alpha - \theta) \\ Z_{sens} &= H - CG_{long}\sin\theta - CG_{lat}sin\phi + D_{bias}\cos\alpha \\ X_{road} &= D_{meas}\sin(\alpha - \theta) + X_f \end{aligned} \tag{1.18}$$

The set of values $X_{road}$ and $Z_{road}$ are fed into the buffer and used to attain preview information for the MPC$_p$. Current values of HPR are obtained from the Kalman filter (KF). For accurate KF estimates, road disturbance information from the preview buffer is input into the KF. This interdependence, coupled with processing delays, created unstable preview dynamics.

For robustness, tire dynamics compensation was done externally from the KF. The free response of a quarter-car model, Equation (1.1), to the buffered road disturbance was used to modify the HPR input to Equation (1.18). Figure 1.7 shows the results—raw preview sensor data is shown in the top plot; buffered and corrected road information is shown in the bottom two plots. The plots denoted "original" (dashed lines) are the output of Equation (1.18) using KF estimates without disturbance information; "Tire Comp." includes tire compensation done external to the KF. Observe the negative bump just after the actual bump (at 4.3 s) in the $Z_r$ plot. The negative impression is removed by accounting for tire dynamics. MPC$_p$ places the most weight on $\dot{Z}_{road}$; in the final plot we see a tremendous improvement over the original $\dot{Z}_{road}$. A more robust solution is to resolve issues encountered when incorporating road disturbance information into the Kalman Filter computation.

### Preview Buffer

Incoming, consecutive road data is not guaranteed to have an equal spacing or even a consistent order. New road information is sorted and stored to the buffer with respect to $X_{road}$. Interpolated data is retrieved for the requested $pH$ for each wheel.

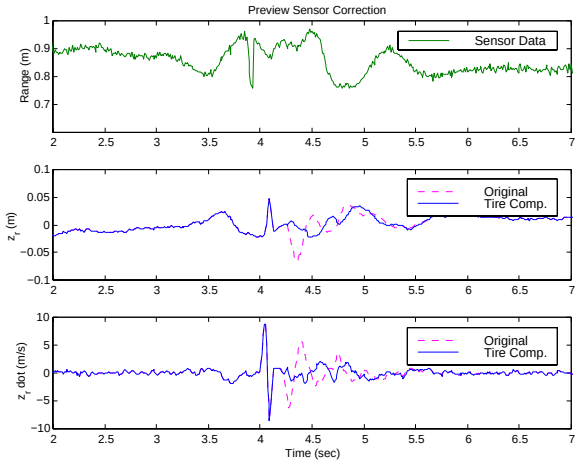


**Figure 1.7** Sample sensor data with HPR correction

The buffer is fixed length, circulating memory. An integer increment in the array pointer corresponds to a fixed increment in the physical distance. Relative distance travelled is maintained by integrating vehicle speed. To improve the stochastic properties of the buffer, new information is interpolated and updated, if necessary, with a forgetting factor.

A standard velocity sensor is used to measure $V_k$ for the experimental HMMWV. In final implementation, an accurate estimation of the ground speed is required to avoid errors introduced by wheel slip, by wheel liftoff, and by loss of traction.

## 1.6 Experimental Results

***Experimental set-up.*** The specially equipped HMMWV (Appendix 1.A) is repeatedly driven over the test track, see Appendix 1.B, at a speed of $20mph$[1]. In subsequent trials, the different higher-level controllers are used. Realistic performance data is collected on an off-road, natural terrain. Prior to system testing, a generated $F_{des}$ profile is fed to the FTCs to verify proper FTC performance; the vehicle is stationary.

***Performance criterion.*** The US Army TARDEC has empirically developed a criterion known as 'absorbed power' to quantify ride comfort. This formulation filters the sprung mass acceleration through a human response filter (HRF) that represents the frequency range most undesirable by a human driver. A second order approximation of the HRF is given in Equation

[1] 20 mph is the limiting speed for a passive suspension. All experiments were conducted at this speed for consistency

(1.19), the units of input acceleration are m/s$^2$. Output from the filter is squared and time averaged over a moving window to produce the absorbed power measure, also known as the cumulative absorbed power (CAP). Over a given terrain the CAP should remain less than 6 W for driver comfort. Drivers inherently slow down when the CAP persistently exceeds the 6 W limit.

$$\widehat{HRF}(s) = \frac{12s}{s^2 + 30.02s + 901.3} \tag{1.19}$$

### Force Tracking Controller

Figure 1.8 depicts nominal FTC performance across the 1 Hz to 10 Hz frequency range as well as the response to a filtered square wave. There is no compensation for model error, Section 1.3, or ORD [10]. If present, ORD would lessen the dip at each square wave peak. Figure 1.8 also shows FTC performance while tracking a discrete $F_{des}$, Section 1.3.

### High-level Controllers

Figure 1.9 depicts typical results. All of the higher-level controllers perform similarly; the MPC is slightly better than the rest. There is a better than twofold improvement in the absorbed power criterion when compared to the passive suspension[2]. LQR and skyhook performance, not shown, are comparable to the MPC performance. This is true provided the system remains within constraints, Table 1.3, and preview information is not used. For the MPC trial, the FTC performance is shown. Observe the two spikes corresponding to the test track bumps (the first bump is larger than the second). At these instances, there is saturation of the control input $u_1$. In theory, the MPC$_p$ reduces the amount of saturation.

Using the controllers off-road, the results of Figure 1.10 are generated. Now, MPC handedly beats the other higher-level controllers. Moreover, the off-road results show that only the MPC maintained a CAP $<$ 6 W. By military standards, this terrain is only drivable at this speed, 20 mph, if the MPC is used. To better understand the improvements of Figure 1.10, the suspension expansion (LVDT) measurements are shown as well. The MPC reduced suspension travel and the likelihood of suspension saturation, which occurs at approximately $\pm$ 0.06 m.

### MPC Preview Controller

Finally, the preview information is added. Only access to the generated preview is available. Figure 1.11 shows MPC verses MPC$_p$ performance for one big bump. There is 15% improvement over normal MPC control. For persistently exciting road profiles this added improvement will greatly improve

[2]Passive suspension is emulated with the hydraulic pump turned off and unpowered spool valves.

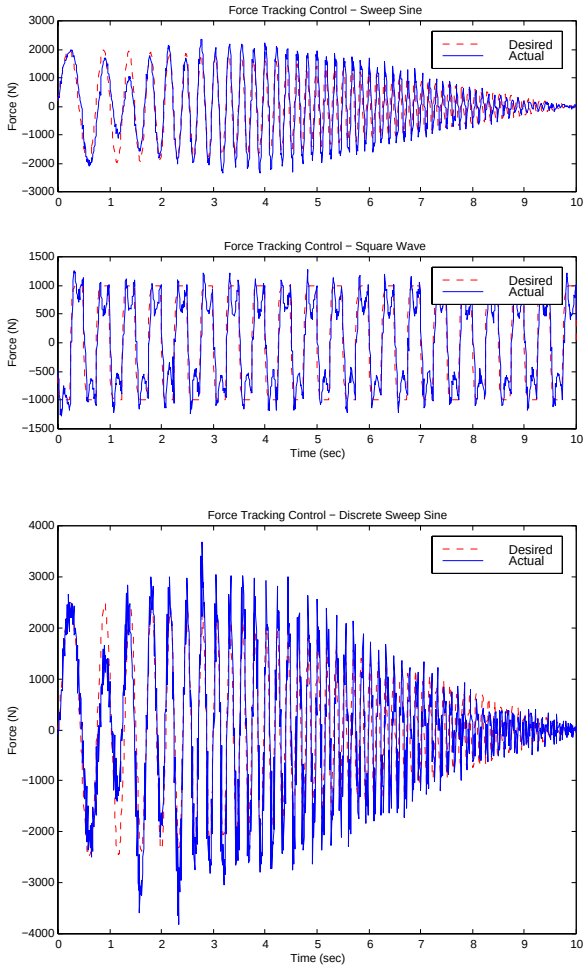


**Figure 1.8** Nominal $FTC$ tracking of generated control signals $F_{des}$. frequency sweep and filtered square wave (*top*) and discrete frequency sweep (*bottom*).

ride comfort. Comparing the preview results with those of Figure 1.9, we see a near threefold improvement over the passive suspension when preview control is utilized.

## 1.7 Conclusions

Practical, implementation-oriented, modifications to dynamic surface control theory were successfully employed. Modifications involved adding filters at various levels of the control computation. To the end of realizing full functionality of model predictive control (MPC) using preview infor-

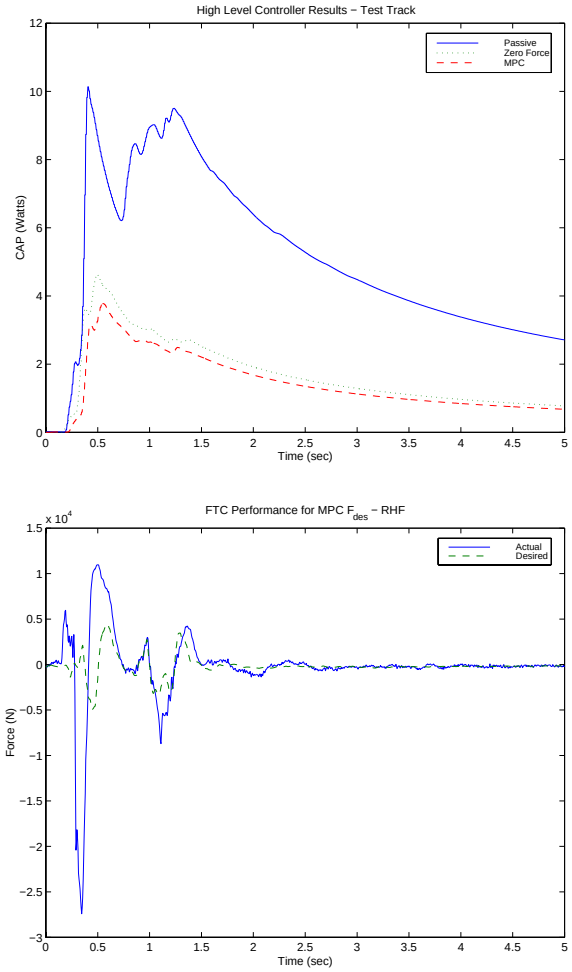


**Figure 1.9** Test track, higher-level controller performance (*top*) and $FTC$ tracking for the MPC $F_{des}$ (*bottom*)

mation, numerous subsystems were designed. All subsystems work well. A skyhook damping controller and a linear quadratic regulator were developed to benchmark the performance of the MPC without preview. For the non-preview controllers, more than a twofold increase in ride comfort over passive suspension was obtained. With preview control, the ride comfort was improved threefold. This resulted in an increased drivable speed for rough terrain. In particular, the MPC allowed for the fastest speed over off-road terrain. All of the infrastructure is in place to use the experimental HMMWV as a test bed for future control algorithms.

Future work is needed on the preview correction algorithm. We feel that

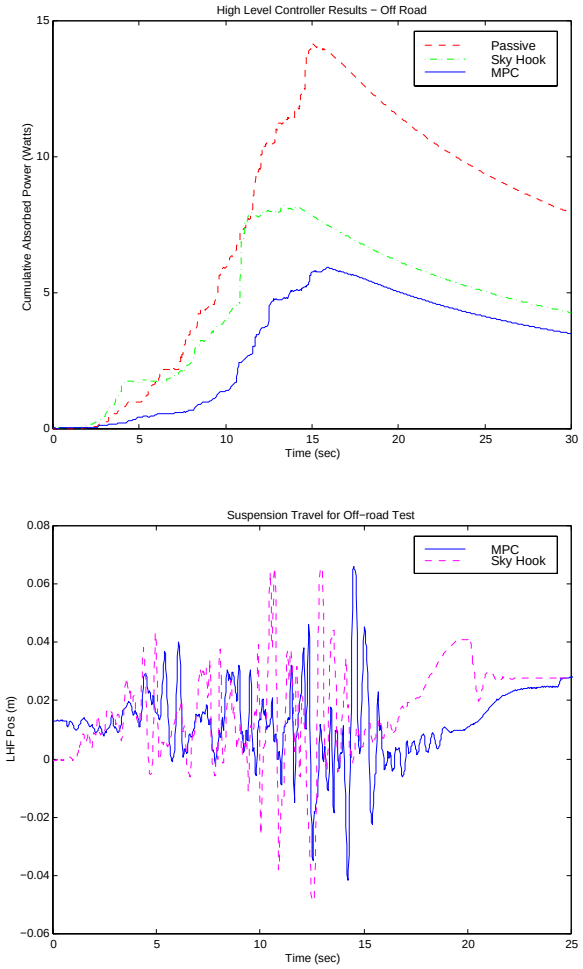


**Figure 1.10** Off-road, higher-level controller performance (*top*) and suspension travels (*bottom*), respectively.

our performance was limited by hydraulic actuator capabilities. Moreover, hydraulics related problems were a nuisance throughout the project. Alternative actuators need be explored for the ultimate realization of the active suspension system.

## Acknowledgments

This work was made possible by the prior research of Professor Andrew Alleyne, University of Illinois at Urbana Champagne, and Carlos F. Osorio of the University of California at Berkeley. The technical support and software expertise of Jayesh Amin from Scientific Systems Company Inc. enabled

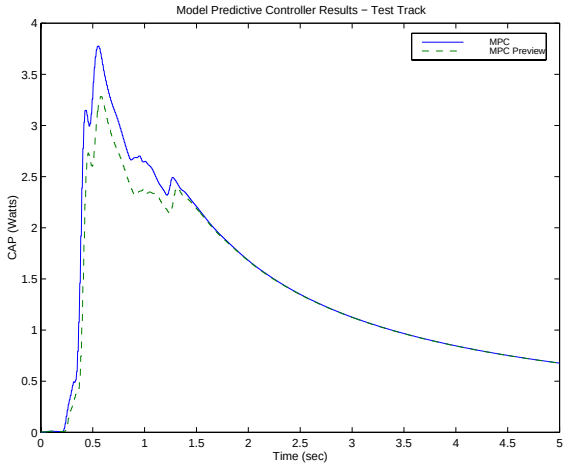


**Figure 1.11** MPC performance using generated preview data

much of the higher-level control theory and implementation. Scientific Systems Company Inc., the SBIR Project Office, and the US Army TARDEC sponsored the project. This work was completed under Phase II of the SBIR contract number DAAE07-96-C-X007.

## 1.8 References

[1] A. Alleyne. *Nonlinear and Adaptive Control with Applications to Active Suspensions*. Ph.D. thesis, Department of Mechanical Engineering, University of California at Berkeley, Berkeley, CA, 1994.

[2] A. Alleyne and J. K. Hedrick. Nonlinear control of a quarter car active suspension. In *Proceedings of the 1992 American Control Conference*, Chicago, IL, 1992.

[3] A. Alleyne and J. K. Hedrick. Nonlinear adaptive control of active suspensions. *IEEE Transactions on Control Systems Technology*, 3(1):94–102, 1995.

[4] A. Alleyne and R. Liu. On the limitations of force tracking control for hydraulic servosystems. *ASME Journal of Dynamic Systems, Measurement and Control*, 1999.

[5] G. H. Engleman and G. Rizzoni. Including the force generation process in active suspension control formulation. In *Proceedings of the 1993 American Controls Conference*, 701–705, San Francisco, CA, 1993.

[6] S. Gopalasamy, J. K. Hedrick, C. Osorio, and R. Rajamani. Model predictive control for active suspensions - controller design and experimental study. *ASME J. Dynamic Systems and Control*, 61:725–733, 1997.

[7] A. Hac. Suspension optimization of a 2-dof vehicle model using stochastic optimal control technique. *Journal of Sound and Vibration*, 100(3):343–357, 1985.

**Table 1.4** Important Vickers PV3-115 hydraulic pump specifications

| Specification | Value |
|---|---|
| Supply pressure | 3000 psi |
| Flow rate | 45 l/min |
| Power consumption | $< 32$ hp at $< 3500$ rpm |

[8] A. Hac. Optimal linear preview control of active vehicle suspension. *Vehicle System Dynamics*, 21:167–195, 1992.

[9] D. Hrovat. Survey of advanced suspension developments and related optimal control applications. *Automatica*, 33(10):1781–1817, 1997.

[10] C. Osorio, S. Gopalasamy, and J. K. Hedrick. Force tracking control for electro hydraulic active suspensions using output redefinition. In *Proceedings of the ASME Winter Annual Meeting*, Nashville, TN, 1999.

[11] R. Rajamani. *Observers for Nonlinear Systems, with application to Automotive Active Suspensions*. Ph.D. thesis, Department of Mechanical Engineering, University of California at Berkeley, Berkeley, CA, 1993.

[12] R. Rajamani and J. K. Hedrick. Observer-based control of an active suspension. In *IEEE Conference on Control Applications*, Dayton, OH, 1992.

[13] R. S. Sharp and S. A. Hassan. The relative performance capabilities of passive, active, and semi-active car suspension systems. In *Proceedings of the Institution of Mechanical Engineers*, volume 203-3 of *D*, 219–228, 1986.

[14] J. J. Slotine and W. P. Li. *Applied Nonlinear Control*. Prentice Hall, 1991.

[15] A. G. Thompson and P. M. Chaplin. Force control in electrohydraulic active suspensions. *Vehicle System Dynamics*, 25:185–202, 1996.

[16] A. G. Thompson, B. R. Davis, and C. E. M. Pearce. An optimal linear active suspension with finite road preview. Paper 0148-7191/80/0225-0520(800520), Society of Automotive Engineers, 1980.

[17] M. Tomizuka. Optimum linear preview control with application to vehicle suspension revisited. *Trans. ASME, J. Dynamic Systems, Measurement and Control*, 98(3):309–315, September 1976.

# 1.A HMMWV Equipment

Lotus Engineering completed original instrumentation of the HMMWV. The University of California at Berkeley added additional sensors and a new computer. Provided below are tables detailing important information regarding the sensor and actuator suites.

**Table 1.5** Essential HMMWV sensors

| Qty | Sensor Type | Location | Measurement |
|---|---|---|---|
| 4 | Load cell | Top mount of each actuator | Actuator forces |
| 4 | LVDT | Inside each actuator | Actuator displacement |
| 4 | Hub accelerometer | On each wheel hub | Axle vertical acceleration |
| 2 | Chassis accelerometer | Opposite corners of chassis | Chassis vertical acceleration |
| 2 | Rate gyro | Center console | Pitch and roll rates |
| 2 | Range | Front of vehicle | Preview, distance to ground |
| 1 | Speedometer | Engine compartment | Vehicle speed |

***Digital signal processing boards.*** The processor suite of choice is the dSpace Autobox components identified below

DS1003: TI TMS320C40 Parallel 60 MHz DSP board
DS1004: DEC Alpha AXP21164 300 MHz DSP board

***Preview sensors.*** For relatively straight path motion or for uniform, wide bumps in the road profile, it is sufficient to use only range finding sensors to obtain preview information. This assumption simplifies the sensor requirements and, as shown in Section 1.5, the preview processing algorithm. Two types of sensors were explored, see comparison in Table 1.6:

1. Frequency modulated continuous wave (FMCW) radar by O'Conner Engineering. The FMCW radar has a central frequency of 24.5 GHz and scanning range of 0.5 GHz.
2. WTA24-P5401 LED optical sensor by Sick Optic. The WTA optical sensor consists of a modulated infrared LED, with an average life of 100,000 hours at 25 $^{o}$C, and precision reflectors all mounted inside a

**Table 1.6** Comparison of HMMWV preview sensors

| Specification | FMCW Radar Nominal Value | WTA24-P5401 Nominal Value |
|---|---|---|
| Range | 1.0 m – 5.0 m | 0.6 m – 1.2 m |
| Resolution | 0.01 m | 0.02 m |
| Light spot | 0.3 m – 0.6 m | 0.02 m – 0.03 m |
| Response time | 1.1 ms | 5.0 ms |

rugged diecast metal housing. The unit meets or exceeds shock and vibration standards: IEC 68-2-27/IEC 68-2-6.

## 1.B Test Track

The HMMWV is stored and tested at the University of California's Richmond Field Station (RFS) in Richmond, CA. The available testing paradigms are: 1) a custom test track, described below, 2) gravel roads, 3) dirt roads, and 4. off-road, grassy terrain. The test track is asphalt to limit the effects of weather, erosion, and wear. We use six standard, hard rubber speed bumps, manufactured by Scientific Developments Inc.. There are 10 possible temporary locations for the bumps along the 32' test region. Bump raisers are used to increase the height of the bumps in 1.5" increments.

## 1.C Nomenclature

| | | |
|---|---|---|
| $A_p$ | Piston area | $0.0044\,\mathrm{m}^2$ |
| $C_{d1}$ | Discharge coefficient | 0.7 |
| $C_{tm}$ | Leakage coefficient $\frac{C_{im}+C_{em}}{2}$ | $15e-12$ |
| $c_s$ | Suspension damping | $12000\,\mathrm{Ns/m}$ |
| $c_t$ | Tire damping | $200\,\mathrm{Ns/m}$ |
| $F_A$ | Actuator force | |
| $F_f$ | Friction force | $120\,\mathrm{N}$ |
| $k$ | Voltage to position conversion factor | $1481\,\mathrm{V/m}$ |
| $k_s$ | Suspension spring stiffness | $240\,\mathrm{kN/m}$ |
| $k_t$ | Tire spring stiffness | $1000\,\mathrm{kN/m}$ |
| $k_v$ | Relative velocity, chassis $\rightarrow$ axle | 2.1 |
| $m_s$ | Sprung mass | $2800\,\mathrm{kg}$ |

| | | |
|---|---|---|
| $m_u$ | Unsprung mass | 270 kg |
| $m_{eq}$ | Equivalent mass $(\frac{1}{m_u} + \frac{1}{m_s})$ | |
| $P_s$ | Supply pressure | 20684 kN/m$^2$ |
| $P_L$ | Pressure induced by load | |
| $u_1$ | Spool valve position | |
| $u_2$ | Bypass valve area | |
| $V$ | Input voltage command | |
| $V_t$ | Total volume of actuator cylinder chamber | |
| $w$ | Spool valve width | 0.008 m |
| $x_s$ | Sprung mass position | |
| $x_u$ | Unsprung mass position | |
| $\alpha$ | Hydraulic coefficient, $4\beta/V_t$ | 2.273$e$9 N/m$^5$ |
| $\beta$ | Bulk modulus of hydraulic fluid | |
| $\rho$ | Specific gravity of hydraulic fluid | 3500 |
| $\tau$ | Spool valve time constant | 0.003 s |